Production of Phenylpyruvic Acid by Engineered L-Amino Acid Deaminase from Proteus Mirabilis

Jia Liu (317320510@qq.com)
Jiangnan University https://orcid.org/0000-0001-8505-2026
Cong Gao
Jiangnan University
Bin Yang
Jiangnan University
Wei Song
Jiangnan University
Guipeng Hu
Jiangnan University
Liming Liu
Jiangnan University
Jing Wu
Jiangnan University

Research Article

Keywords: Phenylpyruvate, L-amino acid deaminase, Product inhibition, Protein engineering, Bio-catalysis.

Posted Date: November 11th, 2021

DOI: https://doi.org/10.21203/rs.3.rs-1045341/v1

Version of Record: A version of this preprint was published at Biotechnology Letters on April 16th, 2022. See the published version at https://doi.org/10.1007/s10529-022-03245-y.

Abstract

Objectives

This study aimed to develop an efficient enzymatic strategy for the industrial production of phenylpyruvate (PPA) from L-phenylpyruvic acid (L-Phe).

Results

L-amino acid deaminase from *Proteus mirabilis* (L-*pm*AAD) was expressed in *E. coli* BL21(DE3) and modified to release product inhibition by employing conformational dynamics engineering. Based on structural analysis, two residues (E145A/L341A) were identified for reducing interactions between the product and enzyme and increasing flexibility of the protein, thereby facilitating the product release. The mutant $M2^{E145A/E341A}$ exhibited a 3.84-fold reduction in product inhibition and a 1.35-fold increase in catalytic efficiency in comparison to the wild type. Finally, 81.2 g/L PPA production with a conversion of 99.6% was obtained in a 5-L bioreactor.

Conclusion

The engineered catalyst can significantly reduce product inhibition and facilitate the effective industrial synthesis of PPA.

Introduction

PPA is widely used in the pharmaceutical, food and chemical industries(Coban et al. 2014; Song et al. 2016). It can be synthesized through hydrolysis and acidification of benzylidene hydantoin (des Abbayes and Salaün 2003) with shortages of expensive precursors, multiple chemical steps and harsh conditions. Thus, developing environmentally friendly biocatalytic methods with amino acids as substrates was desirable (Oike and Groger 2020). The production of PPA via the oxidation of D-phenylalanine by D-amino acid oxidase has been reported. However, this reaction produces toxic hydrogen peroxide and requires additional catalase to remove the toxic effects(Yoshimoto et al. 2014).

L-*pm*AAD has a high catalytic activity for L-Phe (Hou et al. 2016a; Hou et al. 2015). A two-step bioconversion system was previously developed to produce PPA from L-Phe by metabolically engineered *E. coli*, and the total maximal production reached 75.1 g/L in a 3-L bioreactor (Hou et al. 2016b). However, product inhibition was the main limiting factor for resting cell bioconversion, and such two-step bioconversion can also result in multiple byproducts, making extraction and purification of PPA potentially problematic.

Many attempts have been made to carry out site-specific mutations or saturation mutations at the binding sites of products to reduce the interaction with products and thus reduce the inhibition of

products (Atreya et al. 2016). However, such mutations might result in a decrease in catalytic activity or enzyme stability (Atreya et al. 2016). The conformation of the protein plays a key role in enzyme catalysis, including substrate recognition and binding, allosteric regulation, the formation of an enzyme-substrate complex and product release (Han et al. 2016). Conformation adjustment is an effective strategy for protein evolution to reduce product inhibition.

Herein, we engineered the L-*pm*AAD loop structure to reduce product inhibition without decreasing the catalytic efficiency. The best mutant, $M2^{E145A/E341A}$, was identified to increase the flexible conformation in these regions based on structural analysis, thereby facilitating the product release. Finally, the L-*pm*AAD mutants were used to synthesize PPA in a 5-L scale fermenter.

Materials And Methods

Strains and mediums

Cultivation for gene manipulation and plasmid construction was performed in LB broth or on 2% w/v agar plates. Cultivation of *E. coli* cells and enzyme expression for recombinant were performed in the Terrific Broth (TB) medium.

Construction of the L-*pm*AAD mutants

The primers used for gene cloning and pET-20b-*pm*AAD plasmid construction are summarized in Supplementary Table 1. The L-*pm*AAD encoding gene *aad* (GenBank ID: U35383) was inserted into the pET-20b(+) using the restriction sites *BamH*I and *Xho*. The variants were constructed by a whole plasmid PCR protocol using plasmid pET-20b-*pm*AAD as a template.

Determination of kinetic parameters and product inhibition constants

The kinetic parameters were calculated by measuring the initial rates of product formation at different concentrations of L-Phe in Tris-HCl buffer (50 mM, pH 8.0) at 30°C. Samples were analyzed by HPLC. The kinetic parameters were determined by the double reciprocal method(Hou et al. 2016a; Hou et al. 2015).

Molecular modeling and MD simulations

The 3D structural models of L-*pm*AAD and its mutants were constructed based on X-ray crystal structures of the L-AAD from *P. myxofaciens* (PDB ID: 5fjm) by homology modeling. The 3D structure of PPA was downloaded from ChemSpider. Auto Dock Vina 4.0 was used to obtain the staring structure of the L-*pm*AAD in complex with the substrate PPA. The analysis of the structures was performed by PyMOL 2.2. Missing atoms and hydrogen were added to the enzyme using the GROMACS 4.5.5 simulation package. The protonation state of residues was set according to pH 7.0. Na^+ counterions were added to neutralize the system, and the whole system was immersed in a cubic box of TIP3P water molecules, which was extended 10 Å from the dissolved atoms in all three dimensions. MD simulations were performed with GROMACS 4.5.5 and an AMBER03 force field following the three main steps of energy minimization,

system equilibration, and production protocols(Qian et al. 2020). Following steepest-descent energy minimization, 10-ns NVT simulations were run at 300 K in 2-fs. The enzyme and product were assigned to separate energy groups, and the binding energies between them were calculated as total intergroup potential energy(Qian et al. 2020).

Analytical methods

The PPA concentrations were measured by HPLC with an Aminex HPX-87H column. The mobile phase was a 5 mM H_2SO_4 solution at a flow rate of 0.6 mL/min (35°C). L-Phe was determined by automatic pre-column derivatization with *o*-phthalaldehyde using HPLC equipping an FLD detector and an Agilent Zorbax SB-Aq column. The polar eluent was 10 mM KH_2PO_4 pH 5.3 (buffer A) and the nonpolar eluent was a 5:3:1 (v/v/v) mixture of acetonitrile, methanol and 10 mM KH_2PO_4 (buffer B). A flow rate of 1 mL/min was maintained throughout and the column temperature was 40°C.

Fed-batch fermentation

Conditions for obtaining the whole-cell catalyst were performed as described in previous reports (Yuan et al. 2019).

Bioconversion of PPA from L-Phe

The conversion experiments were carried out in a 250 mL shake flask (20 mL working volume) and a 5-L bioreactor (3-L working volume). The 20 mL reaction mixture was incubated at 30ºC and 200 rpm for 20 h. In a 5-L bioreactor, the wet whole-cell catalysts $M2^{E145A/L341A}$ (30 g/L) were added to initiate the reaction. The reaction mixture was stirred at 500 rpm (30 ℃, pH=8).

Results And Discussion

Effect of product inhibition on the synthesis of PPA

L-*pm*AAD was cloned and overexpressed in *E. coli* BL21(DE3) to produce a recombinant strain M0. However, with 70 g/L L-Phe as substrate and 30 g/L whole-cell as biocatalyst, only 42.1 g/L PPA could be produced with a conversion rate of 60.4%. To confirm the product inhibition on L-*pm*AAD, different concentrations of PPA (0-200 mM) were added to the reaction system before conversion. The maximum reaction rate V_{max} values were unchanged, while the K_m values increased along with the PPA concentration, demonstrating a competitive inhibition mode of PPA on the cell bioconversion (Supplementary Table 2).

Directed evolution of L-*pm*AAD by site-saturation mutagenesis

To increase the conformational kinetics of the product binding site and promote the release of the product without perturbing the binding of substrate, the flexible loop regions around the product binding site of L-*pm*AAD were selected for site-saturation mutagenesis. A homology model of L-*pm*AAD was

constructed based on the crystal structure of *P. myxofaciens* LAAD (93.7% identity). The product PPA and cofactor FAD were then docked into the active site of L-*pm*AAD. A total of eight loop regions were identified around the product-binding site (Supplementary Figure 1). Seventeen candidate amino acid residues containing five residues in loop 2 (V411/S412/T414/F415/E417), two residues in loop 3 (T436/V437), five residues in loop 4 (Y97/S98/S102/T105/S106), two residues in loop 5 (D144/E145), one residue in loop 7 (V312) and two residues in loop 8 (L336/L341) were selected for site-saturation mutagenesis.

Then, we substituted the aforementioned candidate residues in the wild-type enzyme (M0) with smaller alanine residues and evaluated the transformed ability of these mutants. As shown in Figure 1, two mutants of $M1^{E145A}$ and $M1^{L341A}$ exhibited 12.1% and 13.3% higher PPA production than the wide type. Therefore, E145A and L341A were combined to construct mutant $M2^{E145A/L341A}$. The PPA concentration of $M2^{E145A/L341A}$ was 1.41-fold higher than the corresponding value for M0. Furthermore, the activities of $M2^{E145A/L341A}$ increased by 210% compared to that of M0 (Table 1).

Table 1
Effect of 70 g/L L-Phe on deamination reaction of mutants.

Mutant	M0	$M1^{E145A}$	$M1^{L341A}$	$M2^{E145A/L341A}$
PPA concentration (g/L)	42.1	47.2	47.7	59.3
Conversion (%)	60.4	67.8	68.5	85.2
Activity (μmol/min/g)	18.5	21.2	25.1	38.9

The kinetic parameters and product inhibition constants of the parent M0 and its mutants were also determined (Table 2). The K_m value of $M1^{E145A}$, $M1^{L341A}$, and $M2^{E145A/L341A}$ was 1.05-, 1.17-, and 1.25-fold higher than the corresponding values for M0, respectively. These mutations seemed to affect the substrate-binding site, resulting in a decrease in the substrate-binding affinity. However, the catalytic efficiency (K_{cat}/K_m) of $M2^{E145A/L341A}$ was 1.62 $mM^{-1}\cdot min^{-1}$, being 1.35-fold higher than that of M0, which was achieved through compensation by the increased K_{cat}.

Table 2
Kinetic parameters and the product inhibition constants of L-*pm*AAD and its mutants.

Enzyme	K_m (mM)	k_{cat} (min^{-1})	k_{cat}/K_m ($mM^{-1}\cdot min^{-1}$)	K_{PI} (mM)
M0	60.4 ± 4.02	72.2 ± 4.04	1.20	119.8 ± 5.91
$M1^{E145A}$	63.8 ± 3.14	80.4 ± 5.12	1.26	289.0 ± 11.8
$M1^{L341A}$	70.4 ± 2.88	94.8 ± 6.89	1.35	354.6 ± 17.8
$M2^{E145A/L341A}$	75.6 ± 3.98	122.4 ± 6.77	1.62	460.0 ± 13.6

Furthermore, the K_{PI} values of $M1^{E145A}$, $M1^{L341A}$, and $M2^{E145A/L341A}$ were 1.41-, 1.91-, and 2.84-fold higher than M0, indicating that product inhibition was relieved. In contrast to conventional random mutagenesis (Hegazy et al. 2019; Wang et al. 2019) or rational mutations that focus on engineering the active site (Atreya et al. 2016), herein, we modified the flexible loop regions around the product-binding site to obtain an effective mutant $M2^{E145A/L341A}$ with a 3.84-fold decrease in product inhibition and a 1.35-fold higher catalytic efficiency than the wild-type enzyme.

Computational evaluation of the mutant M2 $^{E145A/L341A}$

To obtain how the mutation significantly relieves the product inhibition, the relationship between the substituted residues and the surrounding residues was investigated using the AutoDock suite. Based on the structural analysis, the E145 carbonyl group formed a hydrogen bond with the NH_2 group of D149 on loop 5 (Figure 2a), and the L341 carbonyl group made a hydrogen bond with the NH_2 group of L343 on loop 8 (Figure 2c). The prolonged distance between E145 and D149 increased from 1.8 Å to 3.1 Å when the Glu residue at position 145 was replaced with Ala, and the hydrogen bond between them disappeared (Figure 2b). Similarly, when the Leu residue at position 341 was replaced with Ala, the prolonged distance between L341 and L343 increased from 2.8 Å to 3.4 Å, and then the hydrogen bonds disappeared (Figure 2d).

Furthermore, we determined the PPA binding energy of M0 and its mutants. As shown in Supplementary Table 3, the product binding energy of M2 $^{E145A/L341A}$ was 5.0, 2.5, and 1.7 kJ/mol higher than the corresponding values for M0, M^{E145A}, and $M1^{L341A}$, respectively, which was in accordance with the product inhibition relief. Consequently, the surrounding amino acids might improve the flexibility owing to the disappearance of hydrogen bonds, thereby enhancing product release. According to previous studies, higher root-mean-square fluctuation (RMSF) values suggested that these two motifs could undergo noticeable movements and were the most likely to influence protein conformation due to their high flexibility (Han et al. 2016; Yang et al. 2017). A remarkable increase in RMSF around region 1 and region 2 was observed from two substitutions of E145 and L341 as a result of modifying the key amino acid residues (Figure 2e), indicating that the two mutation residues to alanine would thus weaken the structural constraint of the region 1 and region 2, leading to a flexible conformation of L-pmAAD and consequently the opening of the product-binding site. A combination of mutation sites might over-regulate the conformational dynamics and result in low enzyme stability (Han et al. 2016). While the increase in beneficial mutation points was accompanied by an increase in PPA production capacity in this study, probably because single-point regulation had a mild effect on conformation and was within the maximum carrying limit of the conformation.

Synthesis of PPA on a 5-L Scale

To provide a better environment for conversion, the bioconversion parameters, including substrate/whole-cell catalyst ratio, bioconversion pH, as well as temperature, were optimized (Figure 3a-c). Under the optimal conditions (the ratio of substrate/whole-cell catalyst was 2.8:1 in pH 8.5 at a conversion

temperature of 30°C), the titer, yield, and productivity of PPA could reach 81.2 g/L, 99.0%, and 5.1 g/L/h within 16 h in a 5-L bioreactor (Figure 3d), which was the highest titer reported so far (Coban et al. 2016; Hou et al. 2016b).

Conclusion

An engineered L-*pm*AAD mutant with relieving product inhibition for the synthesis of PPA was reported in this study. The product inhibition of L-*pm*AAD was decreased significantly through the enhanced conformational dynamics of the enzyme without a decrease in the catalytic efficiency. The mechanism of relieving product inhibition was discussed based on the analysis of wild-type M0 and its best mutant, $M2^{E145A/L341A}$. Furthermore, the bioconversion performance of mutant $M2^{E145A/L341A}$ was evaluated and 81.2 g/L PPA was produced within 16 h. This represents a significant improvement in the enzymatic production of PPA.

Declarations

Funding This work was financially supported bythe National Key R & D Program of China(2021YFC2100100), theNational Natural Science Foundation of China (22008089),the National First-class Discipline Program of Light Industry Technology and Engineering (LITE2018-08).

Conflict of interest All authors declare that they have no conflict of interest.

Ethical approval This article does not contain any studies with animals performed by any of the authors.

Informed consent Informed consent was obtained from all individual participants included in the study.

References

1. Atreya ME, Strobel KL, Clark DS (2016) Alleviating product inhibition in cellulase enzyme Cel7A. Biotechnol Bioeng 113(2):330-8 doi:10.1002/bit.25809
2. Coban HB, Demirci A, Patterson PH, Elias RJ (2014) Screening of phenylpyruvic acid producers and optimization of culture conditions in bench scale bioreactors. Bioprocess Biosyst Eng 37(11):2343-52 doi:10.1007/s00449-014-1212-7
3. Coban HB, Demirci A, Patterson PH, Elias RJ (2016) Enhanced phenylpyruvic acid production with *Proteus vulgaris* in fed-batch and continuous fermentation. Prep Biochem Biotechnol 46(2):157-60 doi:10.1080/10826068.2014.995813
4. des Abbayes H, Salaün J-Y (2003) Double carbonylation and beyond: systems at work and their organometallic models. Dalton T(6):1041-1052 doi:10.1039/b209103h
5. Han SS, Kyeong HH, Choi JM, Sohn YK, Lee JH, Kim HS (2016) Engineering of the conformational dynamics of an enzyme for relieving the product inhibition. Acs Catalysis 6(12):8440-8445 doi:10.1021/acscatal.6b02793

6. Hegazy UM, El-Khonezy MI, Shokeer A, Abdel-Ghany SS, Bassuny RI, Barakat AZ, Salama WH, Azouz RAM, Fahmy AS (2019) Revealing of a novel xylose-binding site of *Geobacillus stearothermophilus* xylanase by directed evolution. J Biochem 165(2):177-184 doi:10.1093/jb/mvy092
7. Hou Y, Hossain GS, Li J, Shin HD, Du G, Liu L (2016a) Combination of phenylpyruvic acid (PPA) pathway engineering and molecular engineering of L-amino acid deaminase improves PPA production with an *Escherichia coli* whole-cell biocatalyst. Appl Microbiol Biotechnol 100(5):2183-91 doi:10.1007/s00253-015-7048-5
8. Hou Y, Hossain GS, Li J, Shin HD, Liu L, Du G (2015) Production of phenylpyruvic acid from L-phenylalanine using an L-amino acid deaminase from *Proteus mirabilis*: comparison of enzymatic and whole-cell biotransformation approaches. Appl Microbiol Biotechnol 99(20):8391-402 doi:10.1007/s00253-015-6757-0
9. Hou Y, Hossain GS, Li J, Shin HD, Liu L, Du G, Chen J (2016b) Two-step production of phenylpyruvic acid from L-phenylalanine by growing and resting cells of engineered *Escherichia coli*: process optimization and kinetics modeling. PLoS One 11(11):e0166457 doi:10.1371/journal.pone.0166457
10. Oike K, Groger H (2020) Process properties of an l-amino acid oxidase from *Hebeloma cylindrosporum* for the synthesis of phenylpyruvic acid from l-phenylalanine. J Biotechnol 323:203-207 doi:10.1016/j.jbiotec.2020.07.005
11. Qian Y, Lu C, Liu J, Song W, Chen X, Luo Q, Liu L, Wu J (2020) Engineering protonation conformation of l-aspartate-alpha-decarboxylase to relieve mechanism-based inactivation. Biotechnol Bioeng 117(6):1607-1614 doi:10.1002/bit.27316
12. Song Y, Li J, Shin HD, Liu L, Du G, Chen J (2016) Biotechnological production of alpha-keto acids: current status and perspectives. Bioresour Technol 219:716-724 doi:10.1016/j.biortech.2016.08.015
13. Wang X, Jiang Y, Wu M, Zhu L, Yang L, Lin J (2019) Semi-rationally engineered variants of S-adenosylmethionine synthetase from *Escherichia coli* with reduced product inhibition and improved catalytic activity. Enzyme Microb Technol 129:109355 doi:10.1016/j.enzmictec.2019.05.012
14. Yang B, Wang HJ, Song W, Chen XL, Liu J, Luo QL, Liu LM (2017) Engineering of the conformational dynamics of lipase to increase enantioselectivity. Acs Catal 7(11):7593-7599 doi:10.1021/acscatal.7b02404
15. Yoshimoto M, Okamoto M, Ujihashi K, Okita T (2014) Selective oxidation of D-amino acids catalyzed by oligolamellar liposomes intercalated with D-amino acid oxidase. Langmuir 30(21):6180-6 doi:10.1021/la500786m
16. Yuan Y, Song W, Liu J, Chen X, Luo Q, Liu L (2019) Production of α-Ketoisocaproate and α-Keto-β-methylvalerate by engineered L-amino acid deaminase. ChemCatChem 11(10):2464-2472 doi:10.1002/cctc.201900259

Figures

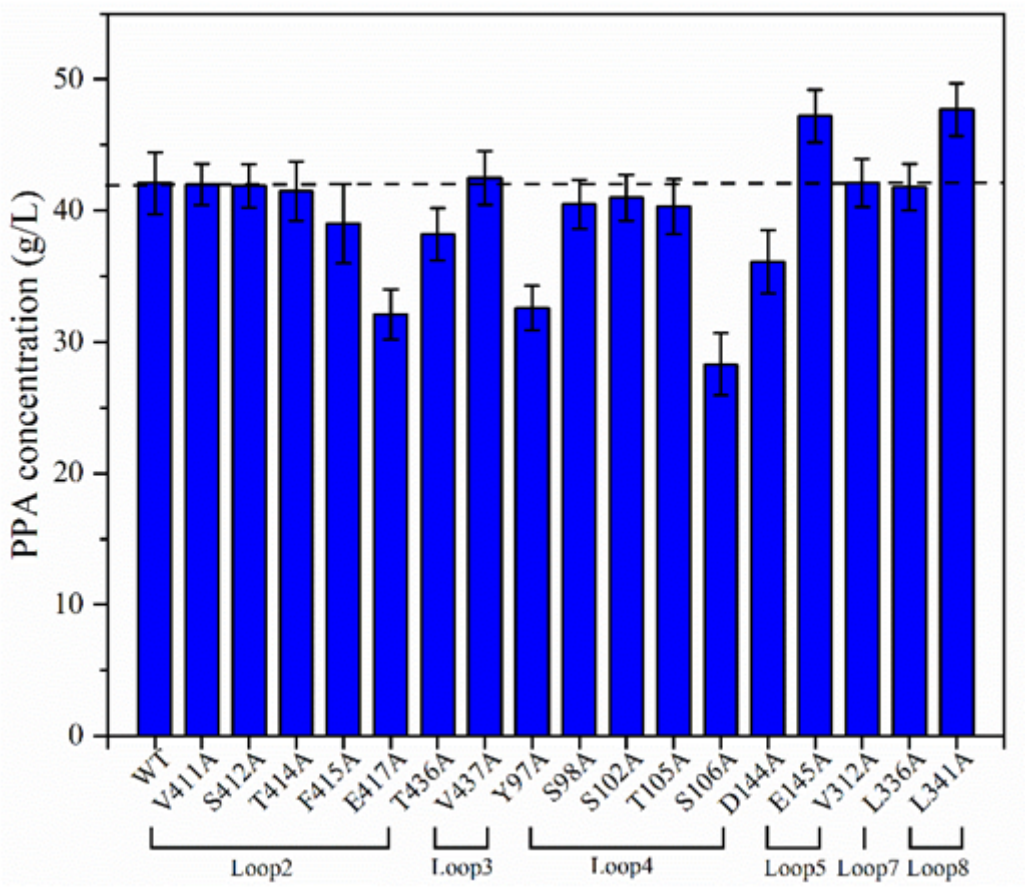

Figure 1

The evaluation of single-mutation variants. The catalytic capability of mutants was determined usinga 30 g/Lwhole-cell catalyst and 70 g/LL-Phe in a 250 mL shake flask. Values are shown as mean ± SD (n = 3).

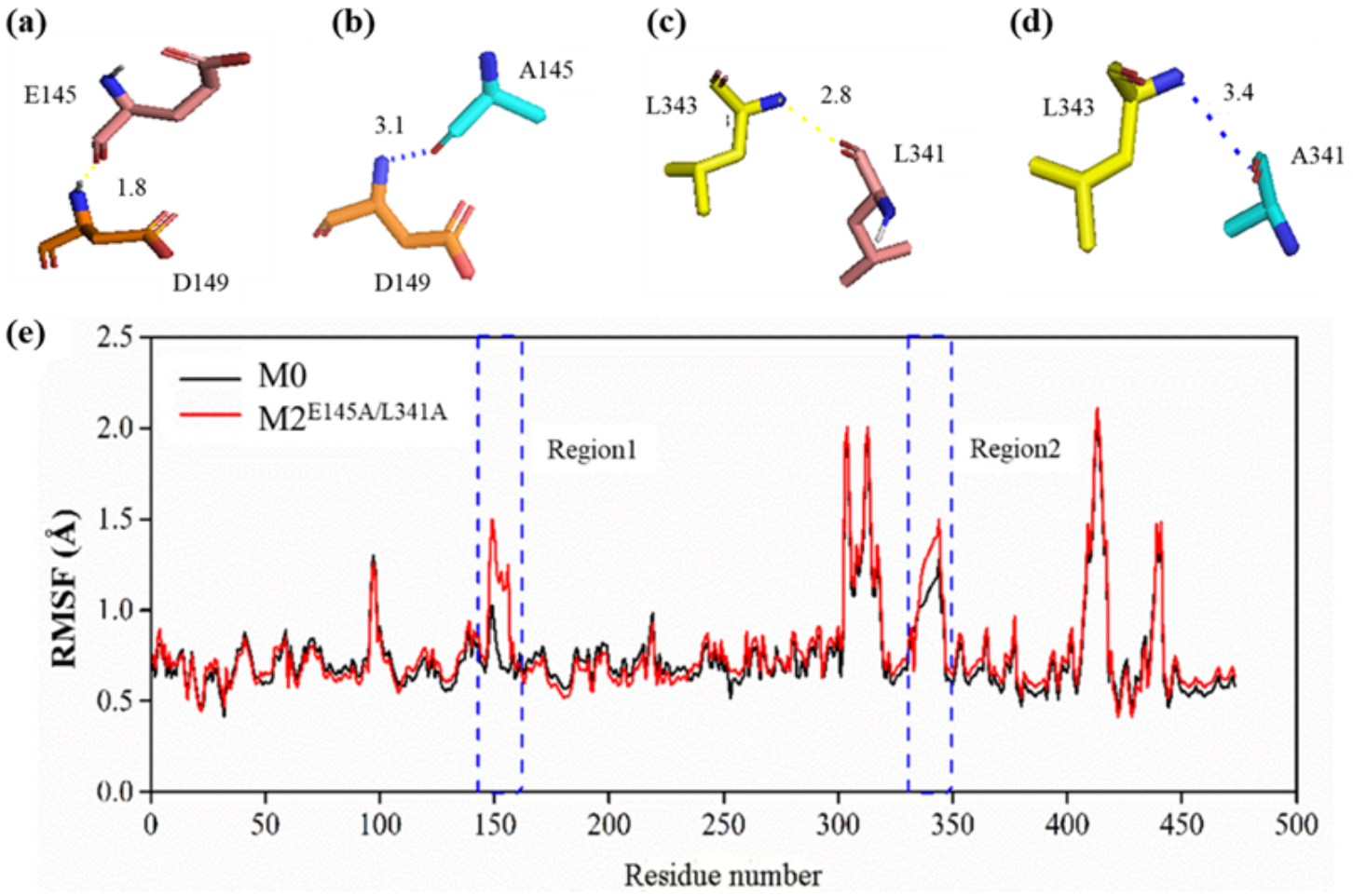

Figure 2

Structural features of M0 and M2E145A/L341A around the mutated residues. (a) E145 with the surrounding residues in wild-type M0 and the mutated residues. (b) E145A with the surrounding residues in M2E145A/L341A. (c) L341 with the surrounding residues in wild-type M0 and the mutated residues. (d) L341A with the surrounding residues in M2E145A/L341A. Red is oxygen and blue is nitrogen. Hydrogen bonds are presented as yellow dashed lines. The disappeared hydrogen bonds in the mutant M2E145A/L341A are presented as blue dashed lines. (e) RMSFs for the M0 and M2E145A/L341Awere calculated from MD simulations.

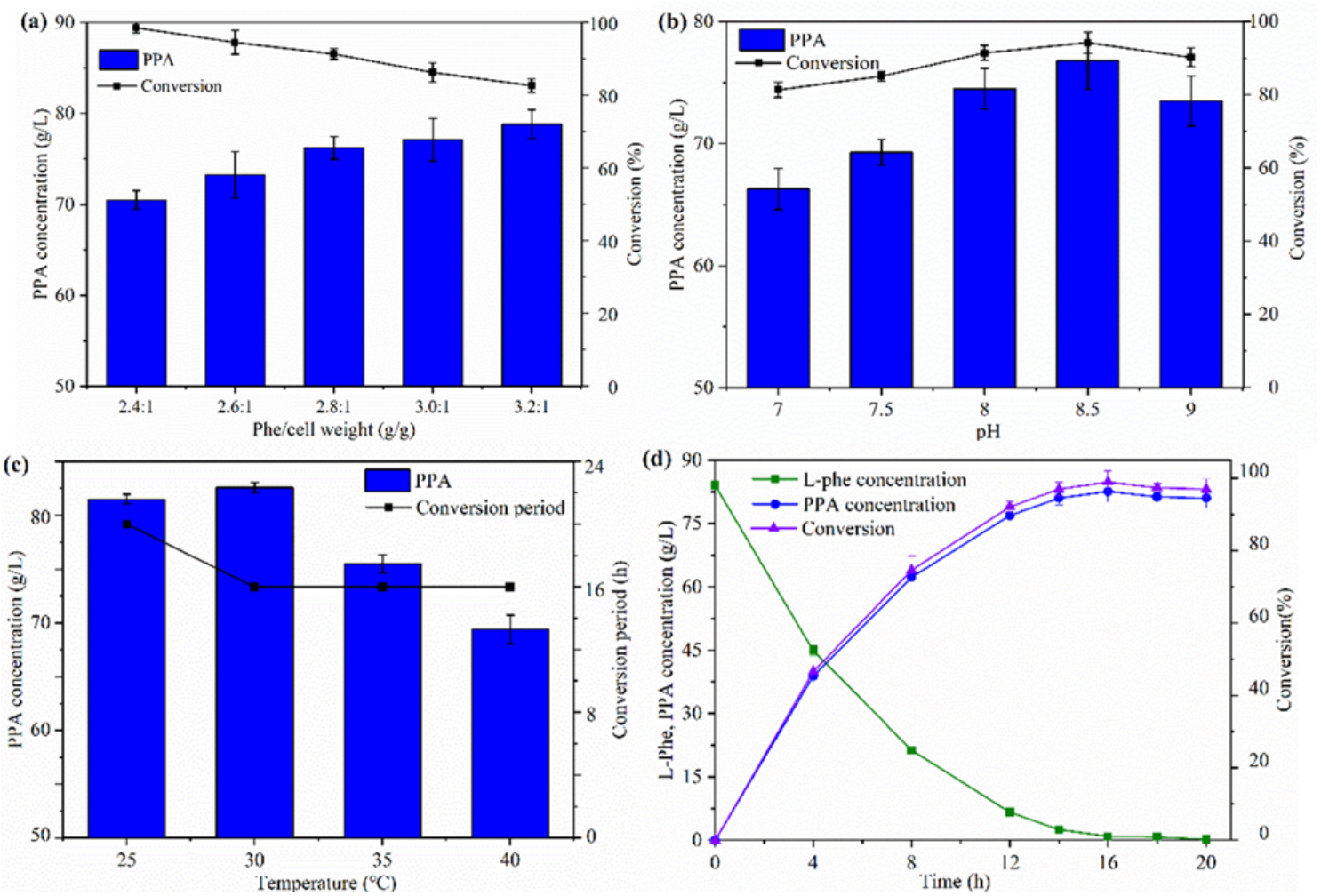

Figure 3

Optimizations during the conversion process by strain M2E145A/L341A. (a) Effect of the substrate/whole-cell catalyst ratio on PPA concentration. (b) Effect of conversion pH on PPA concentration. (c) Effect of conversion temperature on PPA concentration temperature. (d) Time course of the optimized conditions at 5-L scale. Values are shown as mean ± SD (n = 3).

Supplementary Files

This is a list of supplementary files associated with this preprint. Click to download.

- Supplementarymaterials.docx